Volume 1 | Number 1 | Jan 2013 | Pages 1–100

Nanoscale

www.rsc.org/nanoscale

ROYAL SOCIETY OF CHEMISTRY

ROYAL SOCIETY OF CHEMISTRY

www.rsc.org/nanoscale

Lithographically generated 3D Lamella layers and its structural color

Sichao Zhang, Yifang Chen[*], Bingrui Lu, Jianpeng Liu, Jinhai Shao and Chen Xu

S. Zhang, Y. Chen, B. Lu, J. Liu, J. Shao, C. Xu

Nanolithography and Application Research Group, State Key Laboratory of ASIC and Systems, School of Information Science and Engineering, Fudan University, Shanghai 200433, China

Email: yifangchen@fudan.edu.cn

KEYWORDS: e-beam lithography; butterfly wing; photonic crystal; structural color; lamellae layer.

ABSTRACT

Inspired by the structural color from multilayer nanophotonic structures in Morpho butterfly wing scales, 3D lamellae layers in dielectric polymers (polymethyl methacrylate, PMMA) with n~1.5 were designed and fabricated by a standard top-down electron beam lithography with one-step

exposure followed by an alternating development/dissolution process of PMMA/LOR (Lift-off resist) multilayers. This letter offers direct proof of the structural blue/green via the lithographically replicated PMMA/air multilayers analogue to those in real Morphs butterfly wings. The success of nanolithography in this work for the 3D lamellae structures in dielectric polymers not only enables us to deepen the insight of the mysterious blue color by the Morph butterfly wings, but also breaks through the bottle neck in technical development toward broad applications in gas/liquid sensors, 3D metamaterials, coloring media, infrared imaging devices, etc.

1. Introduction

The discovery of the astonishing 3D lamellae layers standing on Morphs butterfly wing-scales by scanning electron microscope [1] has enabled scientist to successfully reveal the essence of the ever mysterious blue color of the wings. So far, substantial amount of basic research has been carried out to understand the iridescence of the blue color from the butterfly wings [2–5], mainly by using real wing scales taken from the Morph butterfly. Physics of the coloring mechanism has been well established [3]. Potential applications have reportedly been demonstrated in optical gas sensors [6–7], pH sensors [8], structured color regulators [9], efficient solar cells [10], anti-counterfeiting labels [11], and high-speed infrared imaging devices [12–13], etc. For the realization of the broad applications, numerous amount of efforts for replicating butterfly wings have been reported. Notably, Saito et al. [14–15] and Chung et al. [16] mimicked the blue color with wide angular viewing by use multilayer deposition of TiO_2/SiO_2 on irregular substructure. Watanabe et al. [17] fabricated replica of Morpho butterfly scales and observed blue color refection by use focused-ion-beam chemical-vapor-deposition (FIB-CVD). Huang et al. [18] and Chen et al.

[19–20] used the real wings as bio-templates to synthesize the 3D nanostructure by metal oxides and reported that the replica can reflect different colors with various lattice constants and refractive indices. Even though, the technical advance is still limited to the use of real butterfly wings as templates for the replications of natural materials through casting [21–22]. Although Aryal et al. [23] and Cui et al. [24] developed top-down approaches for large area nanofabrication of 3D butterfly wing scales, its optical coloration was not been characterized yet.

Lack of reliable and controllable fabrication technique has become a bottle neck for deeper understanding of the colorations as well as further expansion of the research and development toward industrialization. It is widely recognized that the fatal hurdle that fails the standard top-down nanolithography lies in the difficulty in generating the 3D nanoscale lamellae structures as such neither 3D printing nor laser stereo-lithography is applicable.

Recently, this deadlock has just been broken by the authors of this letter. A novel approach for 3D alternating PMMA/air multilayers has been developed based on one-step electron beam lithography combined with alternating development/dissolution [25]. Successful mimicking of the iridescent blue by quasi-multiple reflection through the artificial butterfly wing scale has been demonstrated. Furthermore, green color was also observed from the nanofabricated lamella layers as designed using the established model. This success enables us to not only study the effects of the lamella material and geometry on the blue reflection but also extend the color from blue to other desired ones such as green [25].

This letter describes the details of the technical development as well as the color deviation by the structural regularity, which were not addressed in our earlier publication. The processing reliability of the developed nanofabrication technique is systematically studied. It is believed that

this work lays a promising foundation for further development toward large scale production of the mimicked 3D lamellae layers.

2. Experimental methods:

It is commonly believed that the blue iridescence of the Morpho butterfly wings comes from the so-called quasi multi-reflection by the Christmas-tree like multilayers, as shown in **Figure 1**a [26], which is qualitatively understood as the case where a pair of thin layers (cuticle/air) piles up periodically. Figure 1b-c shows the simplified lamellae structure being tackled in this work. It is formed by a free-standing periodical ridge (consisting of PMMA/LOR pillar and PMMA/Air branch) with a fixed pitch of 1.2 − 1.5 μm. On each ridge, there are aligned lamellae layers as alternate solid cuticle and cuticle-pillar-supported air layers, following that in Morph butterfly wing scales.

2.1 Resists selection

Figure 2 schematically depicts the process flow with one-step electron beam lithography (EBL) to form alternating cuticle/air bilayers. Initially, two resists with different sensitivities were tried to generate a PMMA/Air multilayer. One of them is PMMA for the cuticle lamellae owing to its similar refractive index and excellent transmission rate to visible light. More importantly, its sensitivity to e-beam is relatively low (230 − 500 μC/cm^2) to most of e-beam resists. For the other resist, there is a big variety of candidates including PMMA-MMA copolymer, ZEP, UV-III and SU-8 for their sensitivities lower than PMMA. However, it was found in our work that the sensitivity difference between PMMA and copolymer (and ZEP as well) is not significant enough [27] to create sufficiently large undercuts needed for cuticle/air multilayers. UV-III is, on the other

hand, too sensitive to control. The solvent of SU-8 was dissolvable to PMMA after spin-coating. Finally, the lift-off resist (LOR) [28–32], which is based on polymethylglutarimide (PMGI) platform, came to our mind because it is dissolvable in alkali solution but inert to most organic solvents and acids after being baked around its glass transition temperature (189 ˚C). It is also insensitive to electron beam, meaning that the development of PMMA layer and the dissolution of LOR layer can be carried out independently. Also, LOR has excellent transmittance in visible light and similar refractive index with both PMMA and the cuticle [33]. Therefore, LOR was finally selected to be the relatively ideal resist for creating a clear and controllable undercut between two PMMA layers.

2.2 Structure design

Figure 1c shows the designed 3D nanophotonic structure as a simplified version from the real one in Morpho butterfly wings [26], consisting of the ridge axis pillars formed by PMMA/LOR and the lamellae branches formed by PMMA/air multilayers. The refractive indices of the PMMA (n_{PMMA}=1.50) and LOR (n_{LOR}=1.58) measured by an interferometer has 0.08 difference, whose disturbance to the coloration is one of the issues to be investigated in this work. The major reflection by the visible light is assumed to be from the PMMA lamella branches, which is also to be experimentally verified in this study. The resonant reflection wavelength can be decided by the constructive interference reflection condition:

$$2(n_1 d_1 \cos\theta_1 + n_2 d_2 \cos\theta_2) = m\lambda \ , \tag{1}$$

in which the footnote "1" and "2" denote PMMA and air, respectively, and θ_i is the incident angle. In particular, Equation 1 for m=1 correspond to the case called the first order reflection, which the

reflectivity corresponding to the wavelength reaching the maximum. If an additional relation of Equation [Equation 2]

$$2n_1 d_1 \cos\theta_1 = 2n_2 d_2 \cos\theta_2 = \frac{1}{2}\lambda$$

(2)

is satisfied further, the optical path lengths for PMMA layer and air layer are equal to each other and the reflection from each interface (PMMA to air and air to PMMA) adds together, the multilayer should give the maximum reflectivity, which known as "ideal multilayer". Based on Equation 1 and Equation 2, the thicknesses of the PMMA and LOR layers (same as air layer) were calculated in an attempt to create a quarter-wave stack with a stop-band centre wavelength in blue (480 nm) and green (520 nm) spectral range here. For an ideal multilayer system with the constructive interference at 480 nm of the wavelength, the thickness of the PMMA layer is 80 nm and the air is 120 nm, which means the thickness of the LOR layer is 120 nm. For achieving the green one, the thicknesses of the PMMA layer and LOR layer are 87 nm and 130 nm, respectively. Both 11 layers (5 periods) and 15 layers (7 periods) structures were fabricated for comparison with respect to the reflectivity. Three kinds of exposure patterns, square array, rectangular array and grating as schematically show in **Figure 3** were used to investigate the layout effect on the processing window.

2.3 Nanofabrication of aligned lamella layers

The fabrication process started with the spin-coating of an 80 nm-thick PMMA (MW 350 K) layer on a clean silicon wafer and subsequent oven baking at 180°C for 1 hr. Then, a 120 nm-thick LOR (Lift-off Resist, LOR-1A) layer was spin coated on the top of PMMA layer followed by soft baking at 180 °C for 20 min. This procedure was repeated 5 times (or 7 times) with the finish of an 80 nm-thick PMMA to form a PMMA/LOR "superlattice-like" multilayer (Figure 2a) [34]. For

comparison, quartz substrate was also used. In this case, a 20 nm-thick aluminum was evaporated on the top of the multilayer to eliminate charging effect during e-beam exposure. Electron beam exposures were carried out by an e-beam writer (JEOL 6300 FS; JEOL Ltd., Japan) at 100 kV with the beam-spot size of 7 nm and the beam current of 500 pA. The exposure dose of 800 μC/cm^2 was applied after careful dose tests. The overall patterned area was 1000×200 μm^2 for each kind of exposed pattern.

In the development process, the 20 nm aluminum layer coated on the top of the resists with quartz as substrate was first removed by immersing in 1% (w/w) KOH solution for 120 s. An alternating development/dissolution process was then carried out at 22 °C (Figure 2b-c). For the first 6 periods of PMMA/LOR, the PMMA was developed in MIBK:IPA (1:3) for 60s, followed by the dissolution of the LOR in 40% (w/w) CD-26 solution for the same time length. For the remaining 5 periods as the deeper layers, ultrasonic agitation was added to the development/dissolution process to increase the dissolution rates to both of PMMA and LOR. The ultrasonic agitation should help to reduce the surface tension of the solutions and accelerate the transport of reaction species. A grating-like PMMA/LOR multilayer with slight undercuts was obtained as shown in Figure 2d. To create the undercuts needed for the PMMA/air branches, a 60% (w/w) CD-26 solution was applied to dissolve the LOR layers in between the PMMA layers (Figure 2d-e), assisted by the ultrasonic agitation. The undercut widths were well controlled by the dissolution time.

3. Results and discussion

3.1 Optimization of the process parameters

To achieve the reliable nanofabrication process for the 3D complex lamellae, the processing parameters and the exposure patterns were systematically optimized.

(1) The concentration of the CD26 solution

The concentration of the CD26 solution plays the key role for forming the undercuts in the selective dissolution process of LOR layers buried between PMMA layers. Processing study of the concentration parameter was systematically conducted. Three different concentrations of 100%, 60% and 40% were respectively applied for comparison. For each layer of LOR, the dissolution time was fixed to be 60 s and the temperature as 21°C. **Figure 4** presents the quantitative measurements of the undercut lengths of the resultant lamellae layers via three different process routes. Table 1 summarizes the corresponding lithography results. It was found that pure CD26 was too strong to maintain the LOR layers. On the other hand, 40% CD26 solution was too weak to dissolve the LOR between two PMMA layers for undercuts when it was applied in both developing/dissolution and undercut creation, as shown in column 1 in the table. Although 60% CD26 solution was able to create desired undercuts in the PMMA/LOR multilayer (column 2 in table 1), it caused severe decrease in the undercut lengths from the top to the bottom because the upper layers of LOR received much longer dissolution than the lower ones. The optimal process is presented in column 3 of the table. That is, 40% CD26 should be utilized in the developing/dissolution process and 60% CD26 should be applied to create the undercuts for forming the air layers between PMMA layers.

(2) Dissolution time and the effect of ultrasonic agitation

As described above, the 60% CD26 solution was applied to efficiently dissolve the LOR between the PMMA layers for creating air layers. Furthermore, the undercut lengths can be well controlled

by the developing time, as demonstrated by the SEM images as well as the curves of undercut length vs. dissolution time in **Figure 5**. Once again, the dissolution rates are strongly related to the depth of the LOR layer. The undercut length becomes larger as the dissolution time goes on, until the whole LOR layer was dissolved and the PMMA layer on the top collapsed (corresponding to 3 minutes). Ultrasonic agitation also played an important role in the creation of deep lamellae structures when the total layer number increases to 15. **Figure 6** shows the comparison of the resist profiles with and without the ultrasonic agitation. The agitation assistance in deepening the trenches can be understood that the mechanical vibration promotes the development of the resists by destructing the surface tension and accelerating the exchange of reaction species.

(3) The exposure dose dependence

It was found that the exposure dose affects not only the trench-width (or the ridge-width) but also the undercut length although LOR is not sensitive to e-beam. **Figure 7**a shows the SEM micrographs for the lithographically generated lamellae layers under various exposure dose from 975 to 1600 μC/cm^2. Higher dose gives rise to larger undercut lengths which is also quantitatively presented in Figure 7b. This can be readily interpreted as more exposure dose creates broader trenches (i.e. narrower ridge-width), allowing more alkali solution to dissolve LOR layers.

For the same reason, it was also found that the 2D mesh pattern has limited space such that reaction species are unable to reach deep levels easily, leaving unwanted residual resists on the bottoms. Therefore the mesh pattern was excluded in the further work. Both the rectangular and the grating pattern were finally used.

3.2 Coloration characteristics of the lithography based lamella layers

The coloration of the fabricated lamella layers with free-standing PMMA/air multilayer configuration was optically characterized by spectral measurements in visible wavelength range (350 nm – 750 nm) [25]. **Figure 8** presents the colors observed from the patterned surface by an optical microscope (Zeiss Axio Scope A1) with the white balance carefully adjusted. Both blue and green colors are demonstrated, respectively corresponding to two different sets of thicknesses determined by the multi-reflection model (Equation 1 and 2).

Figure 8c shows the top-down image with 1000× magnification of the optical microscope. The enlarged area shown in Figure 8d unambiguously indicates that the blue color is truly from multilayer reflection [4] by the PMMA/air branches as highlighted by dash-lines. Apparently the fabricated lamellae layers mimics the iridescent blue of the real Morphs butterfly wings very successfully for vertical viewing angle.

As shown in Figure 1, the geometry shape of the fabricated lamellae layers partially differs from the real ones. Firstly, the fabricated one owns strictly flat top in each ridge, whilst the real one exhibits the Christmas tree shape on the top [26]; Secondly, all the ridges in the fabricated one has the same height, but there is about 50 nm fluctuation in the real wings. Thirdly, the two sets of branches supported by each ridge have half pitch misalignment, but the fabricated lamellae layers are precisely aligned. Fourthly, there are spacious cavities in the bottom of the ridges in the real wings but none in the fabricated structures. In addition, there is an difference of 0.08 in refractive index between PMMA and LOR in the LOR/PMMA ridges, in contrast to the real wing structure in which the ridges are made from one material, chitin whose complex refractive index is $1.55+0.06i$ [35]. These distinctions in the structure may result in coloration alteration between the artificial and the real lamellae layers, which can be observed from oblique viewing angles.

The spectra in visible frequency were taken from the patterned areas with lithographically generated lamellae layers of PMMA/LOR branches supported by the PMMA/LOR pillars. The spectra in **Figure 9**a-b were taken from the samples with totally 11 layers, specifically designed for mimicking blue color. Strong reflection peaks in blue region are recorded for either 0 degree or 30 degree incidence of lights. Furthermore, the blue peaks remain unchanged for the viewing angles of roughly ±10 degree, which is narrower than that in the real butterfly wings. This is because of the high regularity in the lithographically generated lamellae layers. Whilst in the real butterfly wings, the "Christmas tree" shape of the ridges, the misaligned branches on the two side of the pillars and the random offset in the ridge heights form the main irregularities, leading to the much broader angle independence of the color [36].

By adjusting the thicknesses in PMMA/air for producing green color, the samples with totally 15 layers (Figure 9c-d) give rise to the reflection peaks in 500 – 550 nm of the wavelengths. Careful comparison between the mimicked blue and the green discovers that the green color maintains unchanged in a wider viewing-angle than the blue one. Optical spectra from the samples with totally 15 layers were also recorded. Increasing the layer numbers is beneficial for enhancing the reflected intensity and broadening the coloring angle.

In this paper, the effect of the periodical change of the refractive index in the PMMA/LOR ridges on the coloration was also theoretically and experimentally investigated. Three different ridges are compared as shown in **Figure 10**a, i.e. grating with single layer of PMMA, PMMA/LOR multilayer ridge array and PMMA/LOR with PMMA/air multilayer branches (the lamellae layers). Figure 10b shows the spatial distribution of the electric field for the wavelength at 524 nm (green color) in three different ridges, simulated by FDTD method. Both the PMMA grating and the PMMA/LOR ridge (without PMMA/air branches) show similar resonant mode existing in the

ridge, giving rise to almost identical reflection. This suggests that the 0.08 alteration between PMMA and LOR hardly influences the reflection. The electric field distribution in the lamellae structure with PMMA/Air branches, however, shows strong reflection due to the multi-reflection by the PMMA/air multilayers. Therefore, our conclusion is that the non-uniform refractive index in the ridges built in the PMMA/LOR multilayers has unobservable effect on the coloration. This can be reflected by both the measured and simulated reflection spectra as shown in **Figure 11**. The simulation result in the figure is extracted from ref [25]. The reflection spectra from both the PMMA grating and the PMMA/LOR multilayer ridge array are not only featureless but also negligible in intensity. Therefore, the designed and fabricated lamellae layers of PMMA/Air supported by the PMMA/LOR ridges can mimic the Morphs butterfly wing structural color closely.

Conclusion

This letter describes in detail about our recent progress in the fabrication of 3D nanophotonic lamellae layers by a standard EBL process with alternating development/dissolution process in PMMA/LOR multilayers. The combination of PMMA/LOR for forming PMMA/air multilayers with large difference in refractive indices is the key to the success for mimicking the blue color of the Morpho butterfly wings. The independent dissolution to LOR without influencing PMMA enables us to create large undercuts between two PMMA layers, which is inapplicable in any other bilayers such as PMMA/copolymer. With optimized process parameters, the lamellae layers as artificial butterfly wings can be repeatedly manufactured. Colorations of both blue and green were successfully demonstrated. Spectral measurements in visible range were carried out to study the effect of the PMMA/LOR ridge on the coloration. Both theoretical and experimental results show that this influence is negligible. The success of nanoscale dielectric lamellae layers by standard

top-down lithography in this work has established a technical background for the application of

structural blue color.

Acknowledgments

References

1 T. F. Anderson, A. G. Richards, *J. Appl. Phys.* **1942,** *13* (12), 748-758.

2 H. Tabata, K. Kumazawa, M. Funakawa, J. Takimoto, M. Akimoto, *Opt. Rev.* **1996,** *3* (2), 139-145.

3 S. Kinoshita, S. Yoshioka, K. Kawagoe, *P. Roy. Soc. B-Biol. Sci.* **2002,** *269* (1499), 1417-1421.

4 S. Kinoshita, S. Yoshioka, *Chemphyschem* **2005,** *6* (8), 1442-1459.

5 L. Plattner, *J. Roy. Soc. Interface* **2004,** *1* (1), 49-59.

6 R. A. Potyrailo, H. Ghiradella, A. Vertiatchikh, K. Dovidenko, J. R. Cournoyer, E. Olson, *Nat. Photonics* **2007,** *1* (2), 123-128.

7 Z. W. Han, S. C. Niu, M. Yang, Z. Z. Mu, B. Li, J. Q. Zhang, J. F. Ye, L. Q. Ren, *Rsc. Adv.* **2014,** *4* (85), 45214-45219.

8 Q. Q. Yang, S. M. Zhu, W. H. Peng, C. Yin, W. L. Wang, J. J. Gu, W. Zhang, J. Ma, T. Deng, C. L. Feng, D. Zhang, *Acs Nano* **2013,** *7* (6), 4911-4918.

9 V. Rossbach, P. Patanathabutr, J. Wichitwechkarn, *Fiber. Polym.* **2003,** *4* (1), 8-14.

10 W. Zhang, D. Zhang, T. X. Fan, J. J. Gu, R. Ding, H. Wang, Q. X. Guo, H. Ogawa,

Chem. Mater. **2009,** *21* (1), 33-40.

11   M. Kolle, P. M. Salgard-Cunha, M. R. J. Scherer, F. M. Huang, P. Vukusic, S. Mahajan,

J. J. Baumberg, U. Steiner, *Nat. Nanotechnol.* **2010,** *5* (7), 511-515.

12   A. D. Pris, Y. Utturkar, C. Surman, W. G. Morris, A. Vert, S. Zalyubovskiy, T. Deng, H.

T. Ghiradella, R. A. Potyrailo, *Nat. Photonics* **2012,** *6* (3), 195-200.

13   F. Y. Zhang, Q. C. Shen, X. D. Shi, S. P. Li, W. L. Wang, Z. Luo, G. F. He, P. Zhang, P.

Tao, C. Y. Song, W. Zhang, D. Zhang, T. Deng, W. Shang, *Adv. Mater.* **2015,** *27* (6), 1077-1082.

14   A. Saito, S.-y. Yoshioka, S. Kinoshita In *Reproduction of the Morpho butterfly's blue:*

arbitration of contradicting factors, Optical Science and Technology, the SPIE 49th Annual

Meeting, International Society for Optics and Photonics: **2004**; pp 188-194.

15   A. Saito, J. Murase, M. Yonezawa, H. Watanabe, T. Shibuya, M. Sasaki, T. Ninomiya, S.

Noguchi, M. Akai-Kasaya, Y. Kuwahara, High-throughput reproduction of the Morpho

butterfly's specific high contrast blue. In *Bioinspiration, Biomimetics, And Bioreplication 2012*,

Lakhtakia, A.; MartinPalma, R. J., Eds. **2012**; Vol. 8339.

16   K. Chung, S. Yu, C. J. Heo, J. W. Shim, S. M. Yang, M. G. Han, H. S. Lee, Y. Jin, S. Y.

Lee, N. Park, J. H. Shin, *Adv. Mater.* **2012,** *24* (18), 2375-2379.

17   K. Watanabe, T. Hoshino, K. Kanda, Y. Haruyama, S. Matsui, *Jpn. J. Appl. Phys.* **2005,**

44 (1-7), L48-L50.

18   J. Y. Huang, X. D. Wang, Z. L. Wang, *Nano Lett.* **2006,** *6* (10), 2325-2331.

19   Y. Chen, J. J. Gu, S. M. Zhu, T. X. Fan, D. Zhang, Q. X. Guo, *Appl. Phys. Lett.* **2009,** *94*

(5), 053901-1-3.

20   Y. Chen, J. J. Gu, D. Zhang, S. M. Zhu, H. L. Su, X. B. Hu, C. L. Feng, W. Zhang, Q. L.

Liu, A. R. Parker, *J. Mater. Chem.* **2011,** *21* (39), 15237-15243.

21   S. H. Kang, T. Y. Tai, T. H. Fang, *Curr. Appl. Phys.* **2010,** *10* (2), 625-630.

22   R. C. McPhedran, A. R. Parker, *Phys. Today* **2015,** *68* (6), 32-37.

23   M. Aryal, D. H. Ko, J. R. Tumbleston, A. Gadisa, E. T. Samulski, R. Lopez, *J. Vac. Sci. Technol. B* **2012,** *30* (6).

24   B. Cui, T. Veres, *Microelectron. Eng.* **2008,** *85* (5-6), 810-813.

25   S. C. Zhang, Y. F. Chen, *Sci. Rep.* **2015,** *5*.

26   P. Vukusic, D. G. Stavenga, *J. Roy. Soc. Interface* **2009,** *6*, S133-S148.

27   Y. F. Chen, *Microelectron. Eng.* **2015,** *135*, 57-72.

28   A. W. McCullough, D. A. Vidusek, M. W. Legenza, M. de Grandpre, J. Imhof, Polydimethylglutarimide (PMGI) Resist - A Progress Report, *Proc. SPIE 0631*, Advances in Resist Technology and Processing III, **1986**, 316.

29   PMGI & LOR Lift-off Resists, http://www.microchem.com/Prod-PMGI_LOR.htm

30   LOR / PMGI Data Sheet, http://www.microchem.com/pdf/RevPMGI-Resists-data-sheetV-rhcedit-100311.pdf

31   J. Golden, H. Miller, D. Nawrocki, J. Ross, Optimization of bi-layer lift-off resist process, http://www.microchem.com/pdf/LOR-Extended-Abstract-Final.pdf

32   PMGI and LOR Resists: FAQs, http://www.microchem.com/pmgi-lor_faq.htm

33   E. D. Palik, *Handbook of optical constants of solids*. Academic press: **1998**; Vol. 3.

34   H. Yabu, T. Nakanishi, Y. Hirai, M. Shimomura, *J. Mater. Chem.* **2011**, 21, 15154-15156.

35   P. Vukusic, J. R. Sambles, C. R. Lawrence, R. J. Wootton, *P. Roy. Soc. B-Biol. Sci.* **1999,** *266* (1427), 1403-1411.

36   R. Siddique, S. Diewald, J. Leuthold, *Opt. Express*, **2013**, 21(12): 14351-14361.
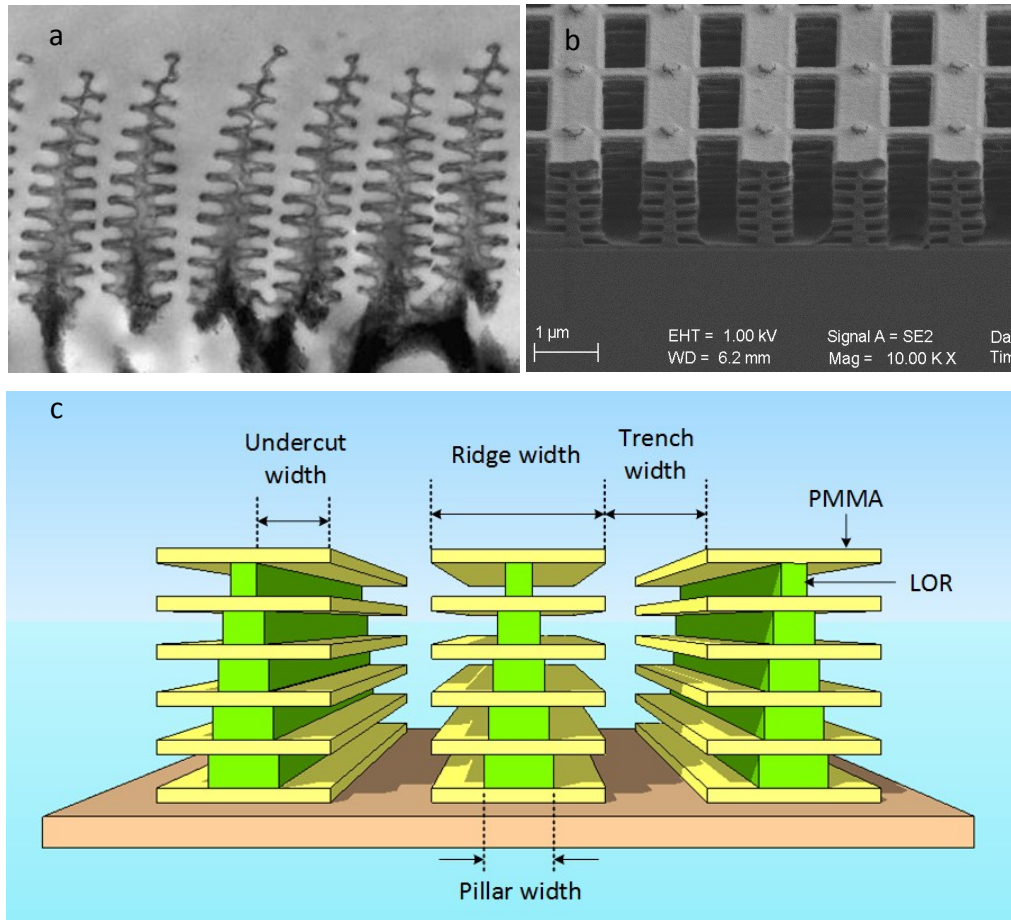
Figure 1. The nanoscale 3D lamellae layers to be studied in this work. (a) The TEM image of the lamellae layers from a real Morpho butterfly wing [26]. (b) The fabricated dielectric lamellae layers. (c) The designed nanophotonic structure with simplified configuration to be manufactured.
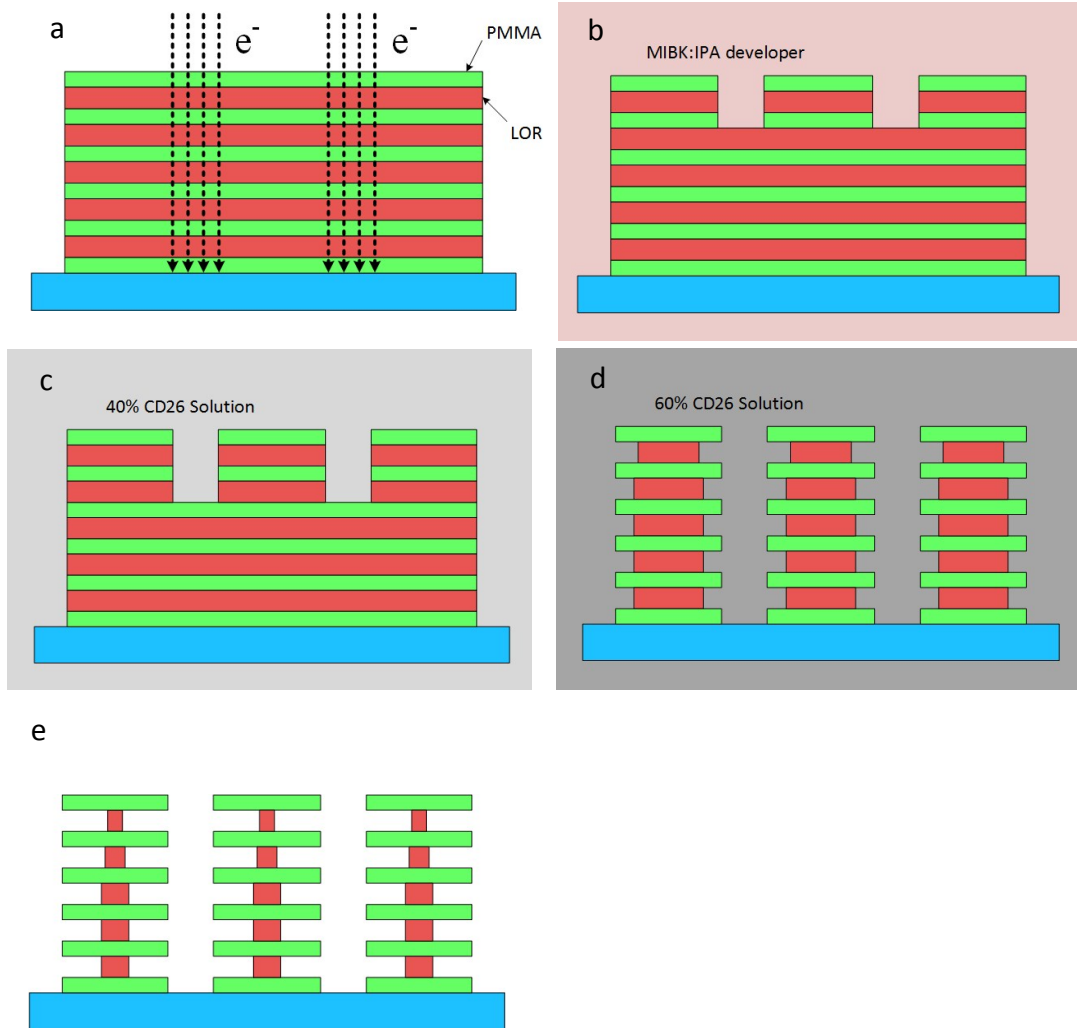
Figure 2. The novel approach invented in this work for the fabrication of nanoscale lamellae layers by stand top-down electron beam lithography, followed by an alternating developing/dissolution process.
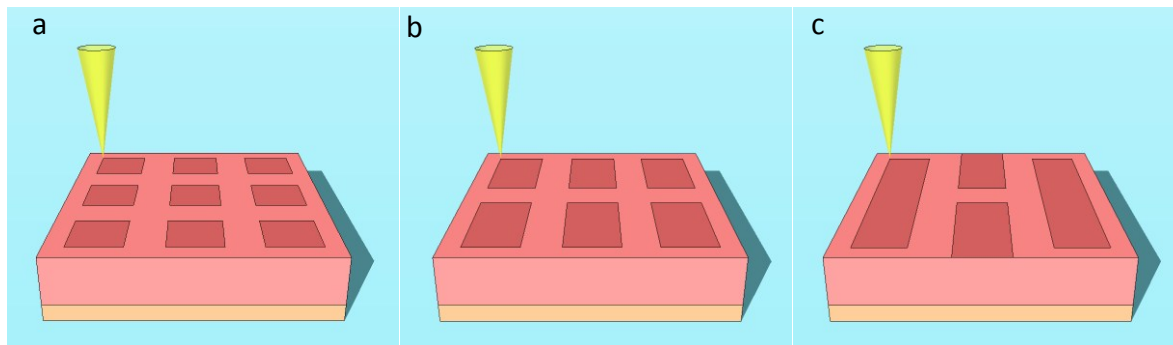
Figure 3. Three different patterns for the e-beam exposure to create ridge arrays. (a) The 0.6 μm×0.6 μm mesh layout with the pitch of 1.5 μm. (b) The 0.6 μm×2.5 μm rectangle array with the vertical gap of 0.9 μm and horizontal gap of 0.5 μm. (c) The grating with exposed lines (0.5 μm)/unexposed space (0.9 μm). Each exposed line has a broken point every 9.5 μm for the mechanical enhancement in the fabricated ridges.
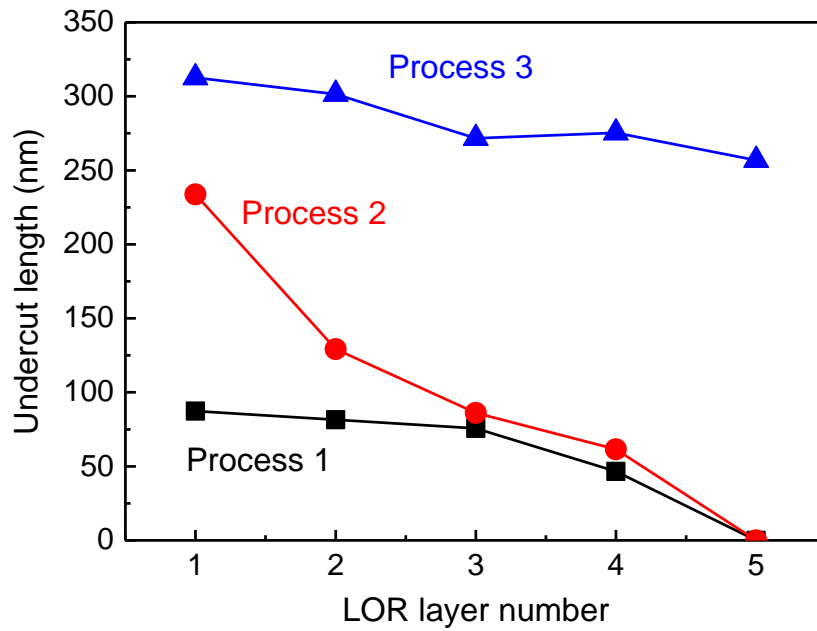
Figure 4. The quantitative measurements of the undercut lengths in the lamellae layers after three different developing/dissolution processes. The processing conditions are summarized in table 1. For detailed description, please refer to the text.

Table 1. Summary of the processing parameters and the resultant profiles by SEM in lamellae

structures.

	Process 1	Process 2	Process 3
Developer of PMMA	MIBK solution	MIBK solution	MIBK solution
Dissolution of LOR	40% CD26	60% CD26	40% CD26
Dissolution for undercut	40% CD26	60% CD26	60% CD26
Resultant profile			
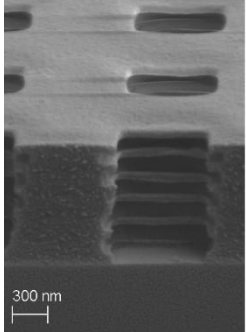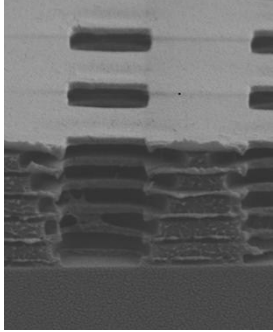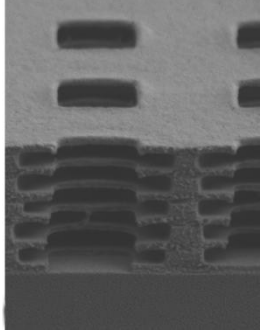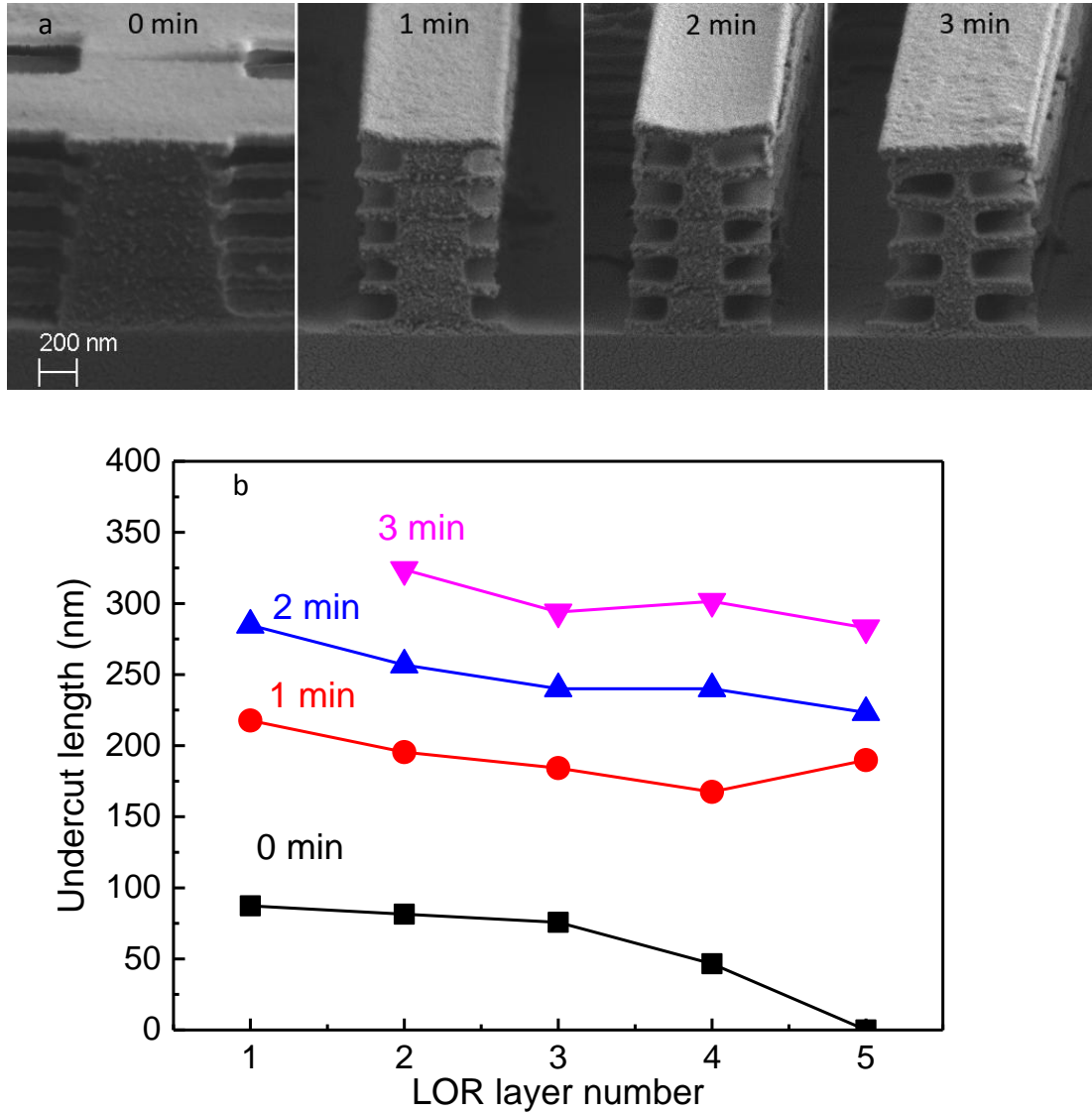
Figure 5. Demonstration of the controllability of the undercut lengths by dissolution time. (a) The SEM images of the lamellae layers after 4 different dissolution time lengths. The dissolution times are marked on the corresponding profiles. (b) The quantitative undercut lengths measured from the SEM photos in (a), showing the good control property.
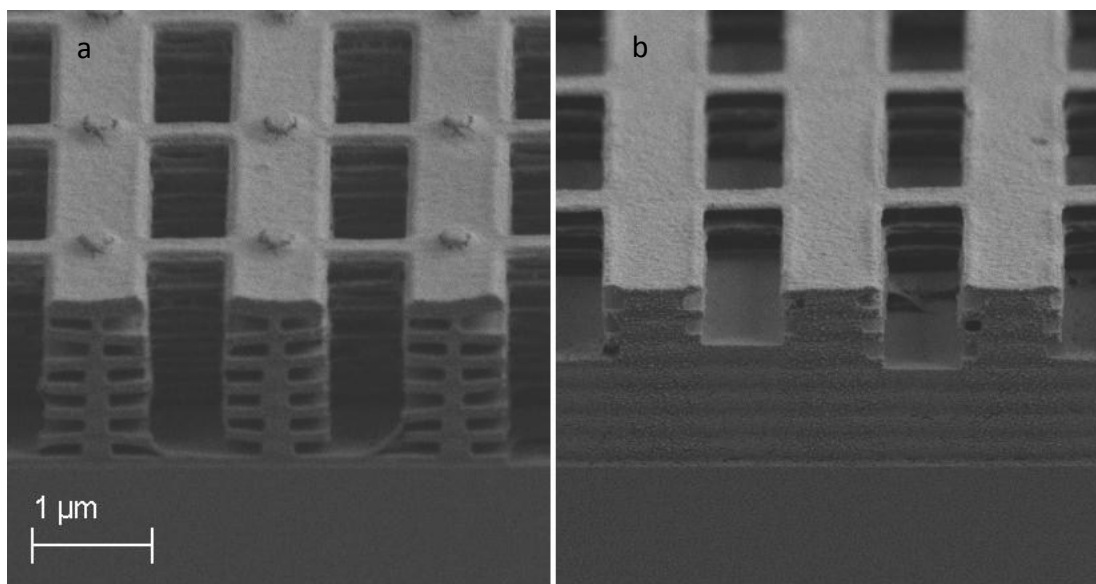
Figure 6. The SEM micrographs of the lamellae layers with (a) and without (b) the assistance of ultrasonic agitation in the developing/dissolution process for the 15 layer sample.
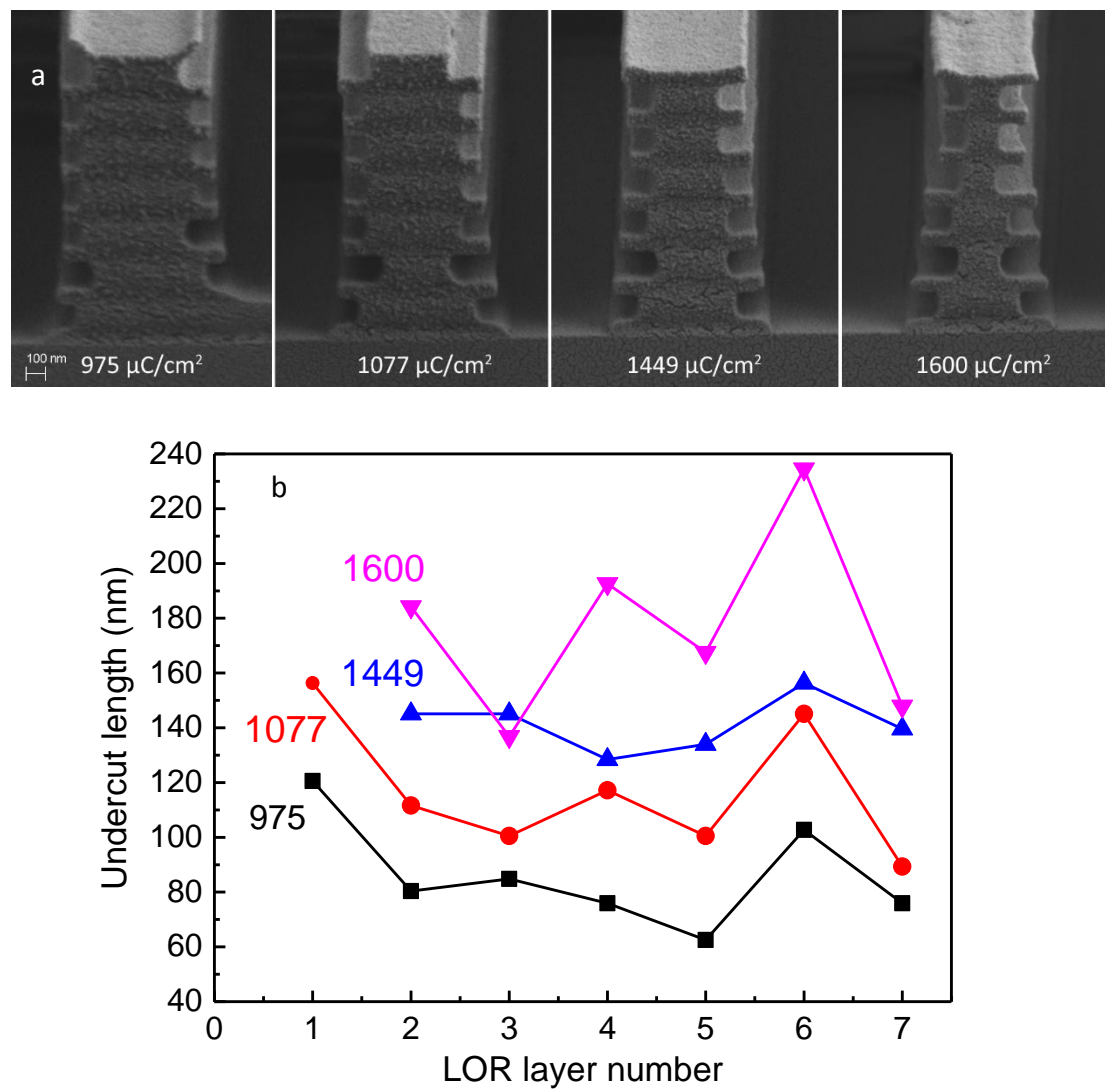
Figure 7. The investigation of the relationship between the undercut length and the exposure dose. (a) SEM micrographs for the lamellae layers under different exposure dose, showing the increase of the undercut and the decrease of the ridge-width by the dose change. (b) The quantitative measurements of undercut lengths. The figures in the plot denotes the dose in the unit of $\mu C/cm^2$.
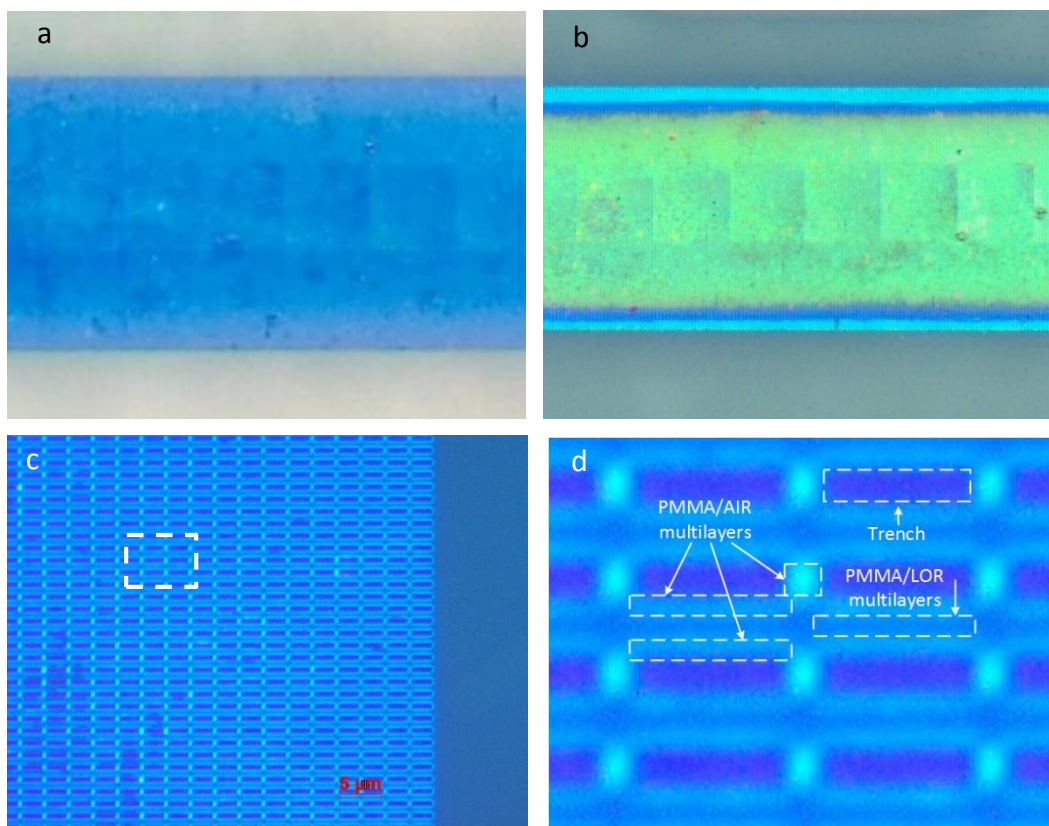
Figure 8. Optical images showing structural colors of both blue (a) and green (b) from patterned areas with lamellae layers. (c) The magnified images from (a) showing the rectangle array detail of the blue color. (d) The close-up view proves that the blue color is truly emitted from the area with PMMA/Air lamellae layers as outlined by the white dash-lines.
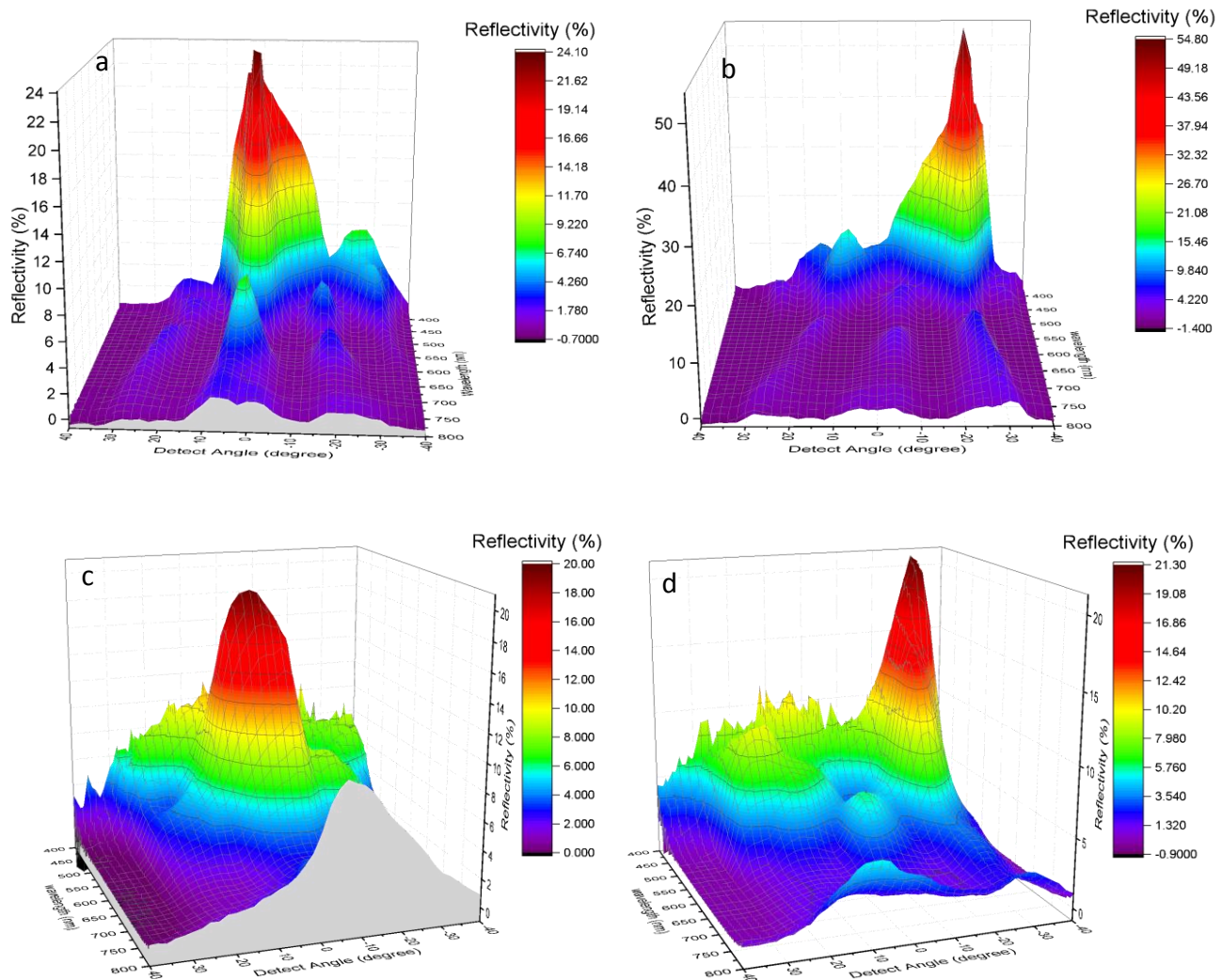
Figure 9. Spectral characteristics of the structural color from the fabricated PMMA/LOR lamellae layers. Angle resolved spectra in visible wavelengths were taken with normal and oblique incidence respectively, to investigate the iridescence of the colors. (a-b) The central color is blue and the incident angle is 0 degree and 30 degree respectively. (c-d) The central color is green with the incident angle of 0 and 30 degree respectively. Detailed description is given in the text.
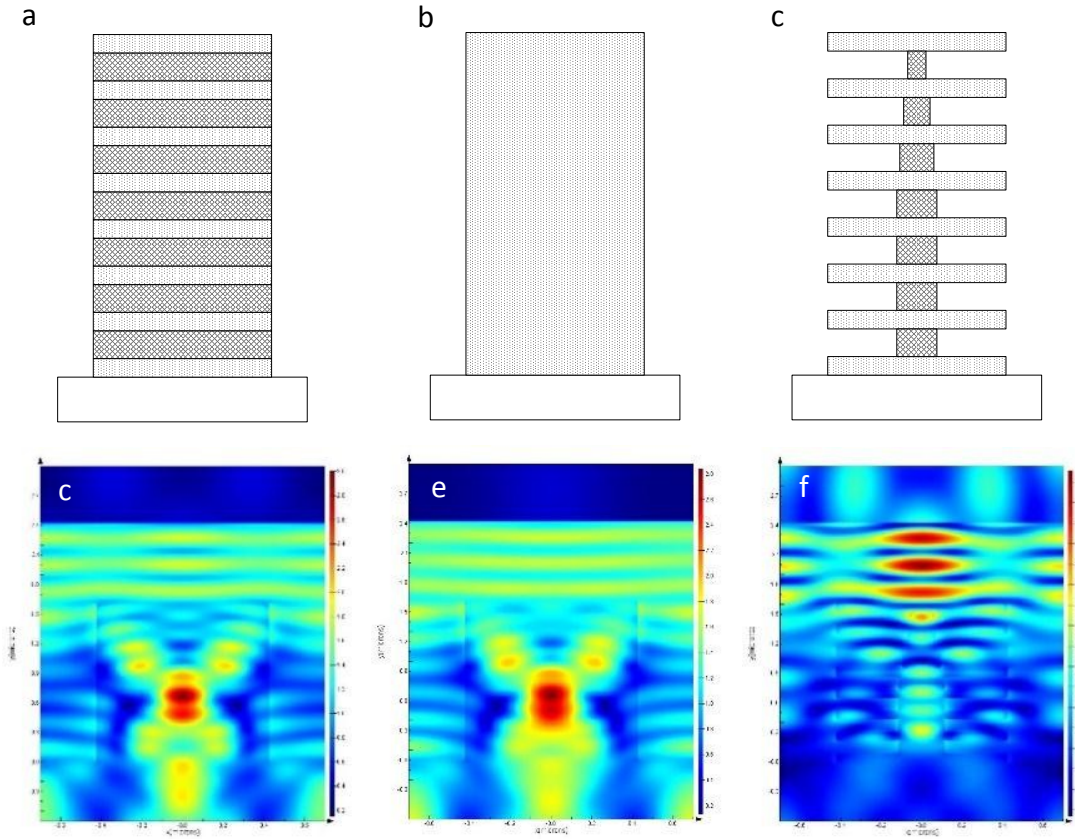
Figure 10. Study of the effect of the refractive index variation in the PMMA/LOR pillar on the structural color. Three different ridges with PMMA/LOR multilayer (a), PMMA single layer (b) and PMMA/Air lamellae layer supported by PMMA/LOR pillars are compared (c). (d-f) The spatial distributions of the electric field for the wavelength at 524 nm (green color) were simulated for the three structures in (a-c), respectively. Both PMMA/LOR pillar array and PMMA grating shows no difference in the waveguide mode inside the structure despite the 0.09 variation in the refractive index along the pillars.

27
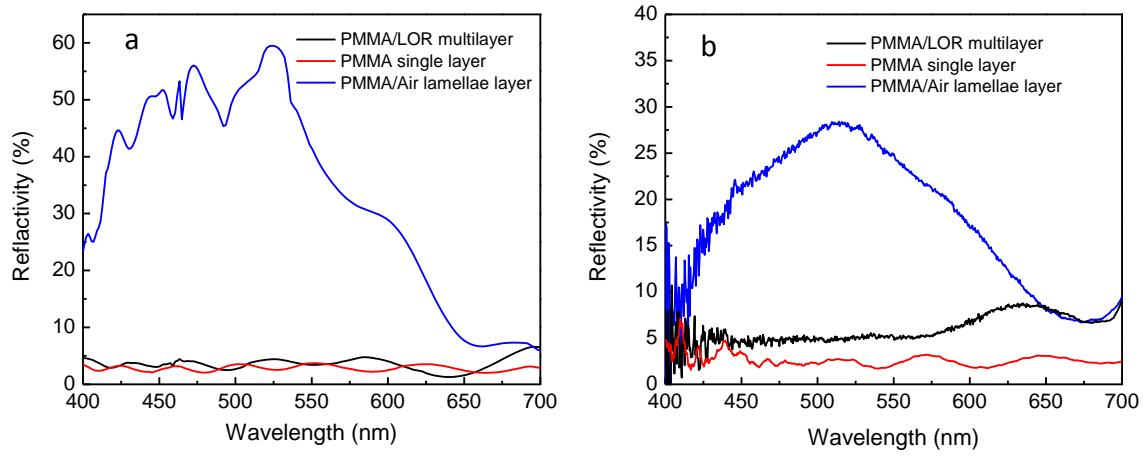
Figure 11. The reflection spectra by both FDTD simulation (a) and measurement (b) from the three photonic structures shown in figure 10. Both theoretical and experimental results verifies that the refractive difference in the PMMA/LOR pillars has negligible influence on the structural color.

This letter offers direct proof of the structural blue/green via the lithographically replicated PMMA/air multilayers analogue to those in real Morphs butterfly wings